Hindawi
Advances in Civil Engineering
Volume 2020, Article ID 6276803, 16 pages
https://doi.org/10.1155/2020/6276803

Research Article

Numerical Investigation on the Influence of In-Plane Damage on the Out-of-Plane Behavior of Masonry Infill Walls

Xiaomin Wang[1], **Weitong Zhao**[2], **Jingchang Kong**[1,2] and **Tiejun Zhao**[3,4]

[1]*Key Laboratory of Earthquake Engineering and Engineering Vibration, Institute of Engineering Mechanics, China Earthquake Administration, Harbin 150080, China*
[2]*School of Civil Engineering, Yantai University, Yantai 264005, China*
[3]*School of Civil Engineering, Qingdao University of Technology, Qingdao 266033, China*
[4]*Cooperative Innovation Center of Engineering Construction and Safety in Shandong Blue Economic Zone, Qingdao 266033, China*

Correspondence should be addressed to Jingchang Kong; kjch8811@126.com

Received 4 October 2019; Revised 20 December 2019; Accepted 28 December 2019; Published 21 February 2020

Guest Editor: Maria T. de Risi

This study presents a finite element model to investigate the bidirectional seismic behavior of masonry infill walls. The test data are utilized to verify the numerical model. The comparison between the analytical and the experimental results indicates that the finite element model can successfully predict the failure mode, stiffness, and strength of the masonry infill wall. Based on the model, the effects of aspect ratio (height to length), slenderness ratio (height to thickness), and masonry strength on the out-of-plane (OOP) response of infill wall with in-plane (IP) damage are explored. Considering the aspect ratio, slenderness ratio, and masonry strength of infill wall, the OOP behavior of infill wall with and without IP damage is studied. Finally the reduction of the stiffness and strength in the OOP direction, due to the IP damage, is discussed.

1. Introduction

Masonry infill walls are frequently adopted as interior partitions and exterior enclosures in RC frame structures. During an earthquake event, masonry infill walls interact with the bounding frames and contribute to the seismic performances of framed structures, often resulting in severe in-plane (IP) damage, out-of-plane (OOP) failure, or even collapse. A large proportion of researches on seismic performance of masonry-infilled frame structures focus on their IP behavior since the infill walls have changed the primary IP load transferring path, which usually results in significant failure of frame structures. However, infill walls are subjected to IP and OOP loads simultaneously. The IP and OOP response are not independent, which means the damage in one direction may influence the response and capacity in the other direction. Therefore, it is necessary to consider the IP and OOP interaction effects to precisely assess the seismic performance of masonry-infilled frame structures.

In last decades, a certain number of experimental investigations, numerical finite element analyses, and theoretical works have been performed. In 1950's, some experimental investigations begin to focus on the OOP response of infill and masonry walls. Thomas [1] and Mc Dowell et al. [2] found out that the arching resistance mechanism forms in masonry walls under OOP loading, which shows that the OOP capacity is dominated by compressive strength rather than tensile strength. Dawe and Seah [3] tested masonry-infilled steel frames under airbag-imposed OOP loads and proposed an OOP capacity model based on the arching mechanism. Dafnis et al.[4] performed shake table tests of masonry-infilled frames in the OOP direction and pointed out that the boundary condition at the top of infill walls has an important effect on OOP response. Similarly, pure OOP tests for masonry-infilled frames are performed by Tu et al. [5, 6].

Angel et al. [7] firstly tested several masonry-infilled RC frames subject to both IP and OOP loads and stated the OOP

capacity is significantly reduced due to IP displacement demand. Based on the arching mechanism, the authors proposed a simplified strength model to account for the IP and OOP interaction effects. Flanagan and Bennett [8, 9] performed a series of tests on masonry infilled steel frames under pure OOP, different sequential, and combined bidirectional loadings to investigate the interaction effects in two directions and proposed a prediction for the OOP strength. Similar experimental studies were also performed by Calvi and Bolognini [10], Kuang and Yuen [11], Pereira et al. [12], Hak et al. [13], and Ricci et al. [14] to further investigate the IP and OOP interaction in infilled RC frames. These experimental programs have demonstrated that the damage in one direction has a detrimental effect on the response of infilled frames in the other direction, and the detrimental effect increases as the damage in one direction increases. To better understand the IP and OOP interaction, a number of experiments were performed to individuate the significant parameters. Angel et al. [7], Ricci et al. [15], and da Porto et al. [16] tested a series of infilled RC frames with different thickness of infill panels to study the influence of slenderness ratio on IP and OOP interaction effects. de Risi et al. [17] investigated the influence of the aspect ratio on the IP and OOP interaction by conducting some masonry-infilled RC frame experiments.

Furthermore, many numerical researches concerning this topic were also carried out. Rabinovitch and Madah [18] and Zhai et al. [19] proposed finite element models for the pure OOP response of infill masonry walls. Mohyeddin et al. [20] and Yuen and Kuang [21] developed 3D discrete finite element models to represent seismic performance of masonry-infilled RC frames under IP and OOP loading. Mohammadi [22] performed a series of numerical analyses to study the effect of IP damage on OOP strength of unreinforced masonry walls. Verlato et al. [23] developed a numerical model of infill masonry walls to carry out parametric analyses for better understanding the main factors influencing the OOP behavior. A nonlinear finite element model was adopted by Agnihotri et al. [24] to consider the influence of slenderness ratio and aspect ratio on IP and OOP interaction. Based on a series of finite element analyses, Zizzo et al. [25] proposed a formulation for the OOP strength reduction factor.

Kadysiewski and Mosalam [26] and Mosalam and Gunay [27] proposed a discrete fiber model to consider the IP and OOP interaction effects of masonry infill walls. Furtado et al. [28] developed a simplified strut model with four struts and two lumped masses for seismic assessment of masonry-infilled RC frames. Adopting the 3D simplified numerical models, the seismic performance of masonry-infilled RC frame structures is analyzed by Mosalam and Günay [27] and Furtado et al. [29]. Di Trapani et al. [30] proposed a macroelement model for IP and OOP responses of masonry-infilled frame structures. Morandi et al. [31] proposed a simplified design approach for masonry-infilled RC frames by taking into account the relation between IP and OOP damage. Pasca et al. [32] reviewed analytical models for the assessment of OOP response of masonry infill walls and examined their suitability by experimental data.

Based on previous studies, it has widely been recognized that the infill slenderness ratio (height to thickness) has a significant influence on the IP and OOP interaction. For equal IP displacement demand, a larger slenderness ratio of infill wall may induce a more severe damage. Meanwhile, at equal IP displacement demand, a larger slenderness ratio decreases the stability of infill walls in the OOP direction, which increases the strength/stiffness reduction and risk of collapse. In addition, the IP response of infill walls is affected by the infill aspect ratio (width to height) too, which may result in different damage levels for infill walls. Moreover, the vertical stability and horizontal stability of infill walls in the OOP direction may change for different aspect ratios. Therefore, the influence of the infill aspect ratio on IP and OOP interaction effects deserves more attention. However, the investigation on the influence of these parameters on the seismic behavior of masonry-infilled RC frames under IP and OOP loads appears to be relatively limited in the existing literatures. Hence, some systematic parametric studies to enhance the understanding level of IP and OOP interaction effects are still needed.

In this paper, a discrete finite element model for masonry-infilled RC frames is described. Then, the influence of different IP lateral drift levels on OOP capacity is studied by using the calibrated finite element model. Different aspect ratios, slenderness ratios, and masonry strengths are considered in the models to evaluate the dependency of these parameters to IP and OOP interaction effects. The results in terms of OOP strength and stiffness reduction for different IP demands are discussed.

2. Finite Element Model

In this paper, a finite element model with a discrete modeling approach is built in ABAQUS/standard module to precisely simulate the nonlinear behavior of masonry-infilled RC frame structures. In this model, appropriate element types and constitutive relationships are selected to simulate the behavior of concrete, reinforcing bars, and masonry blocks. Particularly, contact pairs are utilized to model the cracking and slipping of mortar joints.

2.1. Finite Element Model for the RC Frame. The RC frame is constructed by modeling the concrete members and reinforcement bars separately. The concrete members in the frame are modeled by using 3-D solid elements (C3D8R) with a damaged plastic model as constitutive relationship.

The compression behavior is composed of initial hardening and the following softening section, while the peak strength is followed only by softening behavior in tension. The degradations of the elastic stiffness in tension and compression are independent. Two independent scalar internal damage variables, D_t and D_c, are introduced in the model to characterize the damage of material under tensile and compressive actions. The stress-strain relations are governed by scalar damaged elasticity as follows:

$$\sigma = (1 - d)D_0^{\mathrm{el}} : \left(\varepsilon - \varepsilon^{\mathrm{pl}}\right) = D^{\mathrm{el}} : \left(\varepsilon - \varepsilon^{\mathrm{pl}}\right), \quad (1)$$

where D_0^{el} is defined as the undamaged elastic stiffness of the material, $D^{el} = (1 - d)D_0^{el}$ is the degraded elastic stiffness, and d is the scalar stiffness degradation variable, which can take the values in the range from 0 to 1.

The yield function represents a surface in effective stress space and accounts for different evolution of strength under tension and compression, which determines the states of failure or damage. The yield function takes the following form:

$$\left(\overline{\sigma}, \overline{\varepsilon}^{pl}\right) = \frac{\overline{q} - 3\alpha\overline{p} + \beta\overline{\varepsilon}^{pl}\langle\overline{\sigma}_{max}\rangle - \gamma\langle\overline{\sigma}_{max}\rangle}{1 - \alpha} - \overline{\sigma}_c\varepsilon_c^{pl}, \quad (2)$$

where α and β are the dimensionless material constants, which can be calculated by the ratio of the biaxial to uniaxial compressive strengths and uniaxial tensile stress-strain relation. The parameter γ enters the yield function only for stress states of triaxial compression, when $\overline{\sigma}_{max} < 0$. $\overline{p}$ is the effective hydrostatic pressure, and $\overline{q}$ is the Mises equivalent effective stress. $\overline{\sigma}_{max}$ is the maximum eigenvalue of effective stress tensor in which the notation is the Macaulay bracket. The plastic-damage model assumes nonassociated potential flow, in which the flow potential is the Drucker–Prager hyperbolic function. The uniaxial stress-strain relationship for concrete is defined according to the Chinese code for design of concrete structures (GB50010-2010).

The columns, beams, and slabs are built separately and assembled into an RC frame by using the Tie connect command. Tie connect command is used to realize the binding between different components in ABAQUS, which utilizes "master-slave relation" to define the constraint and prevent the slipping between master and slaver contact surfaces. The reinforcement bars in columns, beams, wall mudsills, and slabs of the frame are all modeled with truss elements (T3D2). A bilinear elastoplastic model with same tensile and compressive capacity is adopted to model the constitutive relationship of reinforcement bars, and the hardening modulus is approximately assumed to be 1.0% of the elastic modulus. The von Mises failure surface with a total stress range of twice the yield stress is assumed for the reinforcing bars. Reinforcement bars are connected to the concrete components by using Embedded command. This connection type has more freedom compared with the Tie command, which allows different components to connect under interferential conditions.

2.2. Finite Element Model for the Infill Wall. To better simulate the cracking and slipping of mortar joints in infill walls, a discrete modeling approach is adopted here, as shown in Figure 1.

In particular, mortar joints between adjacent masonry units are modeled by means of contact pairs, which is realized by defining the contact cohesive behavior, friction behavior, and hard contact to consider the comprehensive behavior of mortar joints. At the initial loading stage, contact cohesive behavior is activated to resist to the tensile and shear forces. Once the strength of contact surface is deteriorated, the stiffness of contact surface is gradually decreasing, and the friction behavior is activated. When

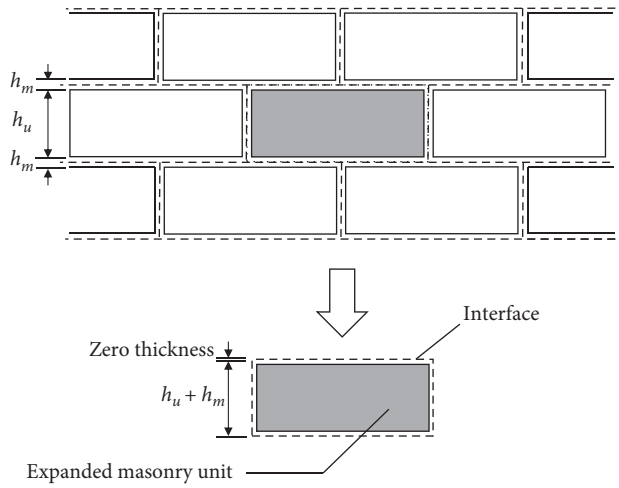

Figure 1: Discrete modeling approach.

cohesive behavior has completely deteriorated, the tensile strength of contact surface reduces to zero, and the friction behavior resists to the shear force. The hard contact is adopted to account for the compressive force and prevent the percolation of adjacent masonry blocks. For the joints at the frame-to-infill interface, contact pairs are also utilized to model the cracking and slipping behavior.

An extended version of the classical isotropic Coulomb friction model is adopted, in which friction factor is a connection between the friction force and compressive normal stress. A friction factor of 0.7 is used according to the Chinese code for design of masonry structures (GB50003-2011). The surface-based cohesive model is established by defining three laws as follows. The linear elastic traction-separation law prior to damage is written in terms of an elastic constitutive matrix:

$$t = \begin{Bmatrix} t_n \\ t_s \\ t_t \end{Bmatrix} = \begin{bmatrix} K_{nn} & K_{ns} & K_{nt} \\ K_{sn} & K_{ss} & K_{st} \\ K_{tn} & K_{ts} & K_{tt} \end{bmatrix} \begin{Bmatrix} \delta_n \\ \delta_s \\ \delta_t \end{Bmatrix}, \quad (3)$$

where t is the nominal traction stress vector, consisting of three components, t_n, t_s, and t_t, which represent the normal and the two shear tractions, respectively. δ_n, δ_s, and δ_t are the associated separations. The interface stiffness K is defined as follows [33]:

$$K_{nn} = \frac{E_u E_m}{h_m(E_u - E_m)},$$
$$K_{ss} = K_{tt} = \frac{G_u G_m}{h_m(G_u - G_m)}, \quad (4)$$

where E_u, E_m, G_u, and G_m are the elastic modulus and the shear modulus of the mortar and the masonry block and h_m is the thickness of the mortar. The other terms in K are assumed to be zero.

Damage initiation refers to the beginning of degradation of the cohesive response at a contact point. The damage initiation criterion is defined as the quadratic stress criterion represented as

$$\left\{\frac{\langle t_n\rangle}{t_n^0}\right\}^2+\left\{\frac{t_s}{t_s^0}\right\}^2+\left\{\frac{t_t}{t_t^0}\right\}^2=1, \tag{5}$$

where t_n^0, t_s^0, and t_t^0 represent the peak values of the contact stress when the separation is either purely normal to the interface or purely in the first or the second shear direction, respectively. The damage initiates when the equation is met. The damage evolution law describes the rate at which the cohesive stiffness is degraded once the corresponding initiation criterion is reached. A scalar damage variable, D, represents the overall damage at the contact point, which evolves from 0 to 1. The contact stress components are affected by the damage according to

$$\begin{aligned} t_n &= \begin{cases} (1-D)\bar{t}_n, & \bar{t}_n \geq 0, \\ \bar{t}_n, & \text{no damage to compressive stiffness,} \end{cases} \\ t_s &= (1-D)\bar{t}_s, \\ t_t &= (1-D)\bar{t}_t. \end{aligned} \tag{6}$$

To keep the overall dimension of the infill wall unchanged, each masonry block and surrounding half thickness of mortar joints are treated as a combined masonry block (as shown in Figure 1) since the thickness of mortar joints cannot be represented by contact pairs. Combined masonry blocks are modeled by using solid elements (C3D8R) adopting a damaged plastic model.

The uniaxial stress-strain relation is defined according to the formulation proposed by Angel et al. [7]:

$$\sigma=\frac{27f_m\left(250\varepsilon_{\mathrm{cr}}-1\right)}{4\varepsilon_{\mathrm{cr}}^3}\varepsilon^3+\frac{27f_m\left(1-333\varepsilon_{\mathrm{cr}}\right)}{4\varepsilon_{\mathrm{cr}}^2}\varepsilon^2+750f_m\varepsilon, \tag{7}$$

where $\varepsilon_{\mathrm{cr}}$ is the crushing strain of the masonry wall and f_m is the compressive strength, $\varepsilon_{\mathrm{cr}}$ is determined as $\varepsilon_{\mathrm{cr}}=1.6\varepsilon_{\max}$. The relation is developed by Liu [34], and $\varepsilon_{\max}$ is the strain at peak strength.

2.3. Verification of the Finite Element Model. In this section, a specimen referred as specimen 2 in the test [7] is utilized to verify the proposed finite element model for simulating the behavior of masonry-infilled RC frames. The specimen is subjected to the combined loading in both IP and OOP directions. The slenderness ratio (height to thickness) of the infill wall is 34, and the detailed geometry and reinforcement information is shown in Figure 2. The material properties for the concrete, masonry blocks, and reinforcement bars are given in Table 1.

The loading mode of numerical analyses is the same as that in the test, and four analysis steps are successively applied. At the first analysis step, self-weight of the specimen is applied and is kept constant during the analysis. At the second analysis step, the vertical load of 241.15 kPa is applied on columns of the RC frame and is kept constant during the analysis. At the third analysis step, the lateral load in the IP direction is applied at the end of beam and with a displacement-controlled procedure. The load is incrementally applied until the interstory displacement ratio (IDR) reaches 0.3% and then the force returns to zero. At the fourth analysis step, the uniform incremental load in the OOP direction is applied on the surface of the infill panel to simulate the airbag loading until the OOP failure has occurred.

The comparison of damage patterns for OOP loading between numerical and experimental results is reported in Figure 3. The damage pattern at the final state of the experiment is shown in Figure 3(a), and it indicates that the crack distribution under IP loading is mainly located at the extremities of the two columns and the beam, whereas stair-stepped diagonal cracks are observed in the infill panel under OOP loading, and an arching mechanism is formed. Figure 3(b) shows the equivalent plastic strain nephogram obtained from finite element analysis, and it illustrates that the damage in the frame has occurred at beam-column joints and bottom of columns. The damage of the infill panel at the OOP direction is characterized by stair-stepped diagonal cracks. In general, a good agreement in terms of damage patterns between finite element analysis and experimental result is achieved.

The IP lateral load-displacement curve obtained from finite element analysis is compared with the corresponding curve from the experimental result, as shown in Figure 4(a). It is illustrated that the initial IP stiffness of the experimental result is slightly larger than that of the analysis result. As the load increases, however, brittle fracture in mortar joints of the infill panel is observed in the experiment, and only compressive stress and friction act, which results in an abrupt reduction of the IP stiffness. In the finite element analysis, the cohesive stress between masonry units is set to gradually decrease as the load increases. Therefore, a smooth load-displacement curve is obtained and no abrupt reduction in the IP stiffness is observed. In general, a good agreement in terms of overall trend, especially at a later stage, is achieved. Figure 4(b) gives the OOP load-displacement curves, and it shows that the initial stiffness and ultimate load from the analysis have a good match with that of the experimental result, while the yielding stiffness from the analysis is slightly larger than that of the experimental results.

The values of initial stiffness and ultimate load in both the IP and the OOP directions obtained from finite element analysis and experimental result are listed in Table 2. The IP secant stiffness at the cracking load of the infill panel is chosen as the initial IP stiffness, and the OOP secant stiffness at 20% of ultimate load is chosen as the initial OOP stiffness. As the OOP load is conducted by only controlling the amplitude of the OOP pressure of the wall, the descending branch of the load-displacement curves cannot be captured. Thus the ultimate load in this paper is corresponding to the load at the OOP displacement of 50 mm.

The error of initial IP stiffness between finite element analysis and the experimental result is 3.7%, whereas the error of ultimate load is only 0.6%. In the OOP direction, the error in initial stiffness estimate is 5.0%, and the ultimate

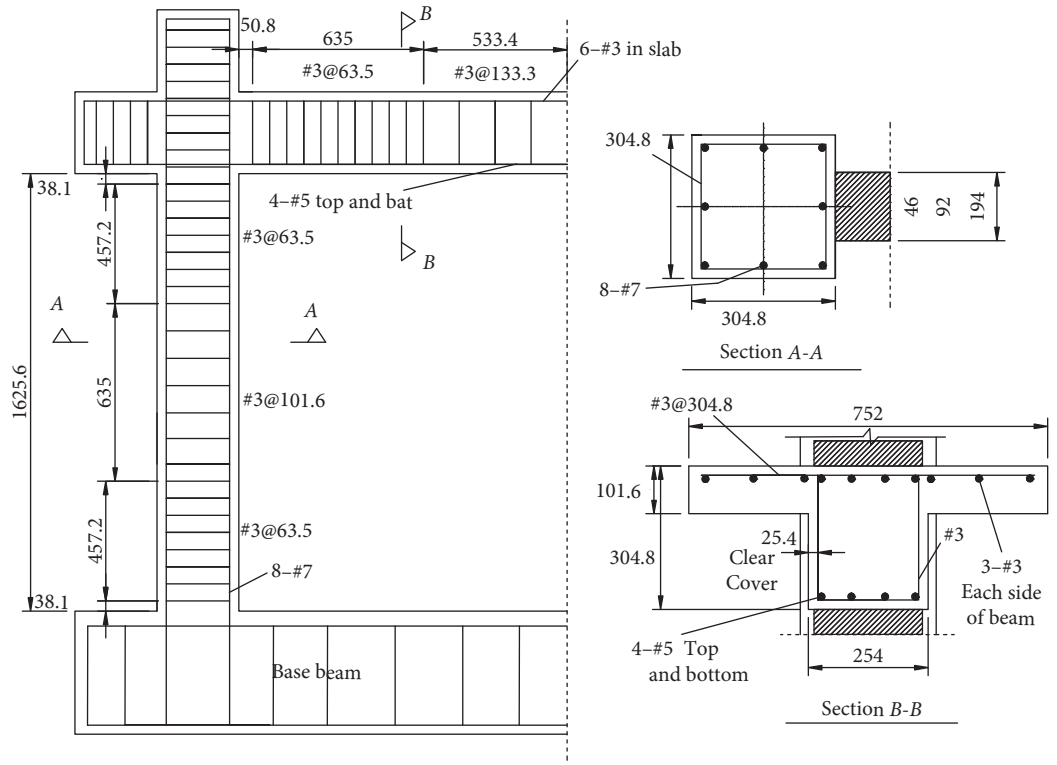

Figure 2: Geometry and reinforcement information (mm).

Table 1: Material properties.

Material	Compressive strength (MPa)	Elastic modulus (MPa)	Tensile strength (MPa)	Reinforcement bars	Yielding strength (MPa)	Ultimate strength (MPa)
Concrete in frame	55	2.8×10^4	2.05	#3	452	731
				#4	457	666
Concrete in wall mudsills	27.5	2.0×10^4	2.05	#5	488	760
Masonry	10.9	8.2×10^3	0.3	#7	457	700

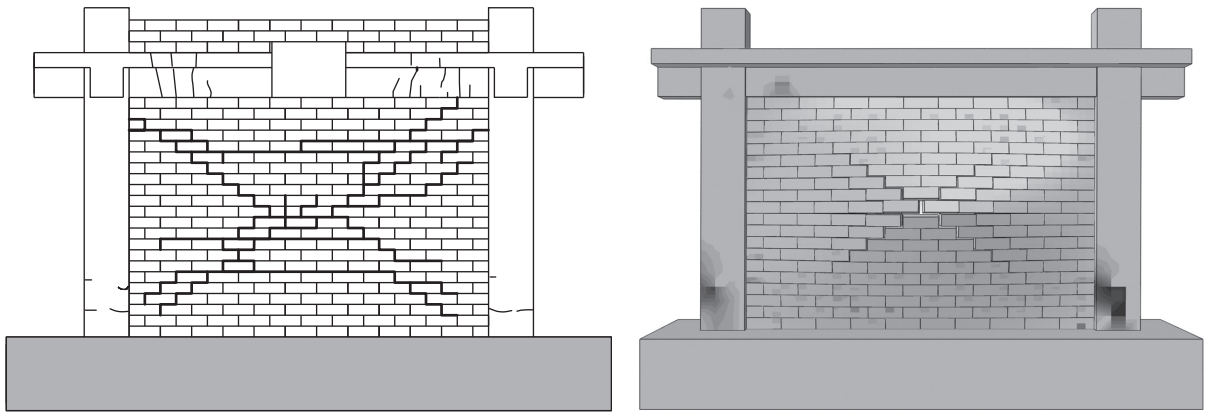

(a) (b)

Figure 3: Damage patterns for (a) experimental and (b) numerical results.

load for the analysis is equal to that of the experimental result. Based on the above comparison, it can be concluded that the finite element model with discrete modeling approach can be used to accurately simulate the nonlinear behavior of masonry-infilled RC frame structures under both IP and OOP loads.

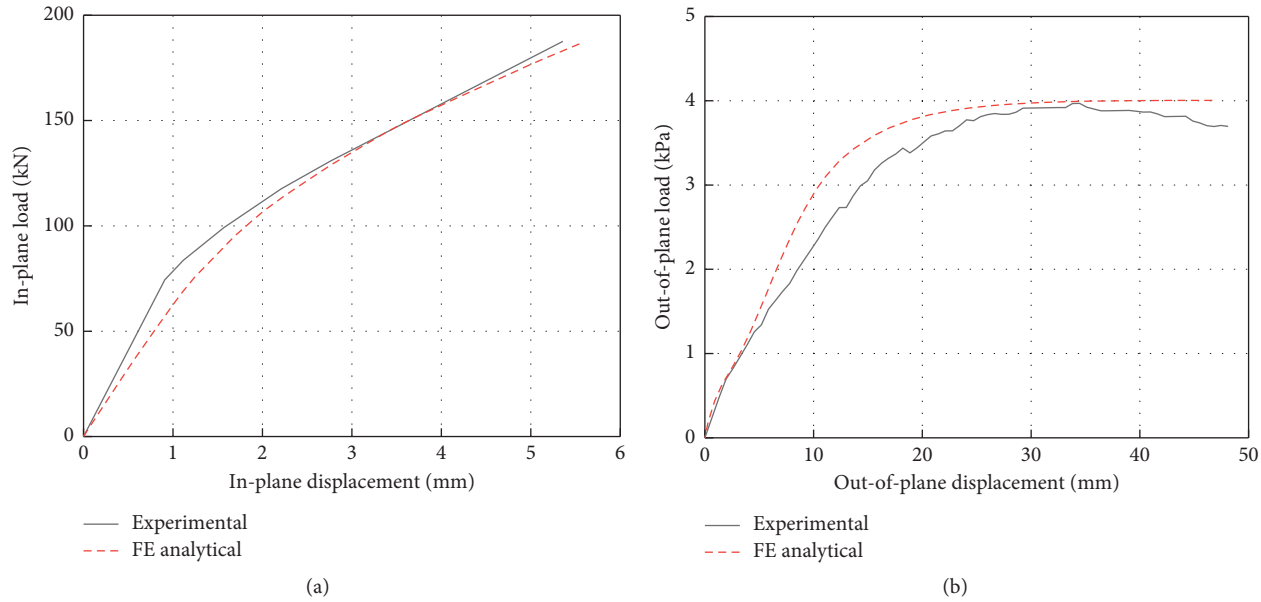

Figure 4: Load-displacement curves in (a) IP and (b) OOP directions.

Table 2: Comparison of numerical and experimental results.

		Initial stiffness (kN/mm)	Ultimate load (kN)
IP	Analysis	33.7	187.6
	Experiment	35.0	186.4
Error (%)		3.7	0.6
OOP	Analysis	319.2	4.0
	Experiment	336.0	4.0
Error (%)		5.0	0

2.4. Sensitivity Analysis for the Finite Element Model. A sensitivity analysis has been conducted to investigate the stability of the numerical results to the modeling parameters used to describe the behavior of the masonry-infilled RC frames. The purpose of the analysis is to identify the most influential parameters and assess the reliability of nonlinear finite element modeling in view of the expected uncertainties in the modeling parameters.

This study considers the modeling parameters used for describing the behavior of the infill walls and cannot be easily obtained from the material tests. The selected parameters are varied, one at a time, to a lower and a higher value, and the range of variation reflects the level of uncertainty associated with the value of the respective parameter. The parameters considered in the study and their bounds of variation are summarized in Table 3 and Figure 5(a). The verified numerical model for specimen 2 is used as the baseline.

To quantify the influence of these parameters on the structural response, the ultimate load and initial stiffness are adopted as the structural response quantities. The percentage change of a response quantity (Q) with respect to the baseline value (Q_B) when the value of a parameter (P) is increased or decreased is used to represent the variation amplitude, which can be described as

$$C_{Q,P} = \pm \max \frac{Q - Q_B}{Q_B} \times 100\%. \quad (8)$$

In addition, the sensitivity of a response quantity to each parameter is obtained from the following formula:

$$S_{Q,P} = \max \left| \frac{Q - Q_B}{Q_B} \frac{P_B}{P - P_B} \right|. \quad (9)$$

Figures 5 and 6 show the percentage change and sensitivity of the structural response quantities, respectively. As shown in Figures 5(b) and 6(a), the percentage change and sensitivity of the ultimate load are not significant for the parameter values considered, except for the variation of the mortar interface shear stiffness perpendicular to the infill panel. In Figures 5(c) and 6(b), the percentage change and sensitivity of the initial stiffness for the variations of parameters considered are presented. The initial stiffness is most sensitive to the interface shear stiffness in two directions. Therefore, the values of these two parameters are not expected to vary considerably. In the modeling, these two parameters are set to the same value and to match the behavior of shear tests.

3. Parametric Analysis

In this section, the influence of IP damage on the OOP seismic performance of infill walls, with different aspect ratios and slenderness ratios, is investigated, using the calibrated numerical model as a reference. The effects of the aspect ratio and slenderness ratio on the OOP behavior of infill walls with IP damage are analyzed.

3.1. Effect of the Aspect Ratio. Infill walls with three different aspect ratios (height to width, H/L) of 0.44, 0.66, and 1.33 are analyzed, respectively, obtained by altering

Table 3: Variation of values for modeling parameters.

Parameter type	K_{nn} (N/m)	K_{ss} (N/m)	K_{tt} (N/m)	Friction factor μ	Fracture energy G^{I} (N·m)	Shear fracture energy G_s^{II} (N·m)	Shear fracture energy G_t^{II} (N·m)
Variation of parameter	1*e*7	1.5*e*7	1.5*e*7	0.5	7.5	75	75
	1*e*8	1.5*e*8	1.5*e*8	0.7	15	150	150
	1*e*9	1.5*e*9	1.5*e*9	0.9	30	300	300

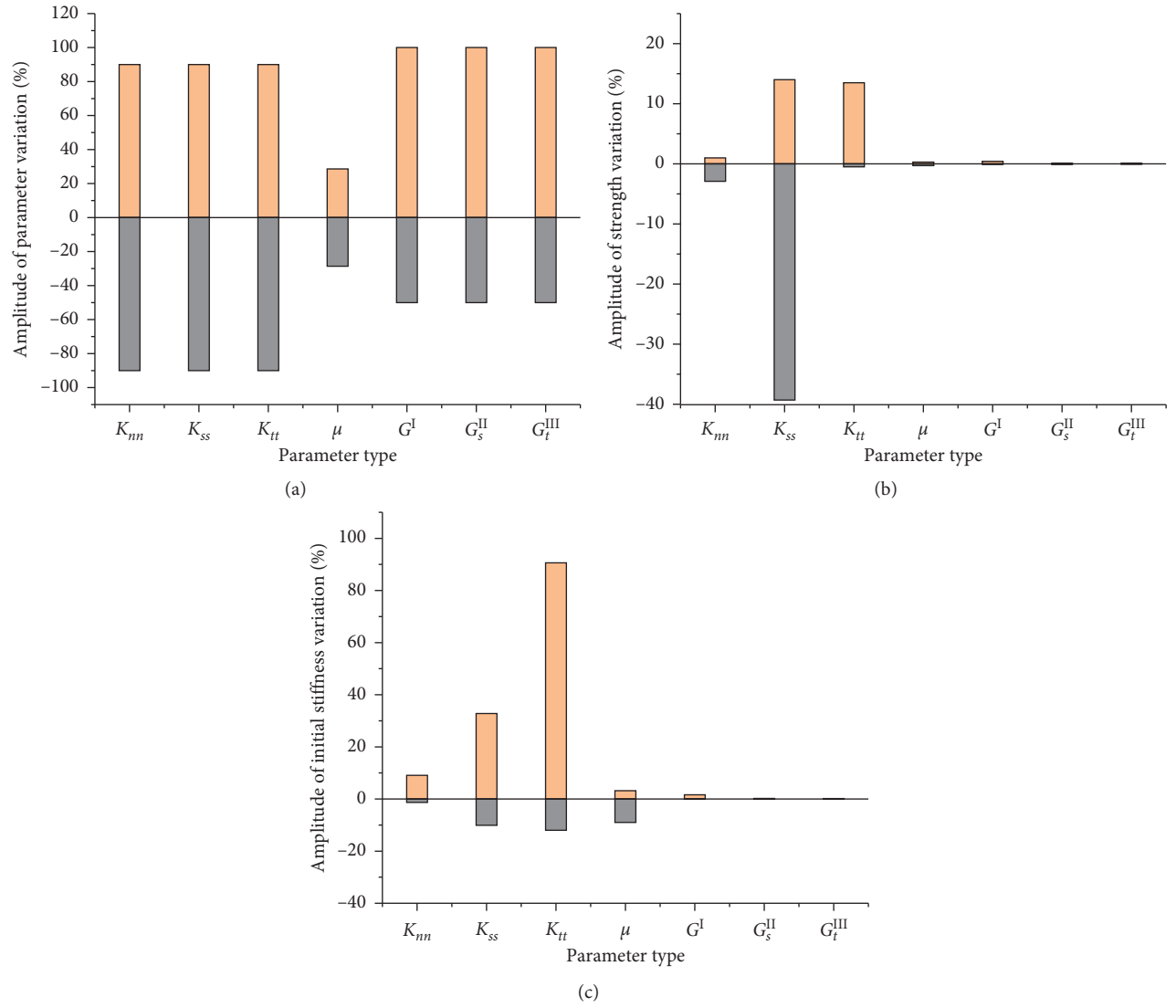

Figure 5: Percentage change of modeling parameters and structural response. (a) Parameter variation. (b) Ultimate load. (c) Initial stiffness.

the width of the infill wall. The height and thickness of all infill walls are 1625 mm and 58 mm, respectively. Detailed information for each analysis model is listed in Table 4. For each aspect ratio, three analyses with different IP damage levels are conducted. It should be stated that the damage level in this study is defined as the maximum IDR. The first is loaded in the OOP direction without any IP damage. The other two correspond to OOP loading, with the IP-IDRs of 0.3% and 0.7% have been first reached, respectively. Thus, nine analyses are conducted.

The ultimate load is corresponding to the load at OOP displacement of 50 mm. The stiffness is computed at the point corresponding to 20% of the ultimate load. The obtained stiffness and ultimate load are listed in Table 4. The OOP load-displacement curves for each analyzed infilled model are described in Figure 7.

3.2. Effect of the Slenderness Ratio. Infill walls with three different slenderness ratios (height to thickness, H/T) of 17, 26, and 34, are analyzed, respectively, obtained by altering

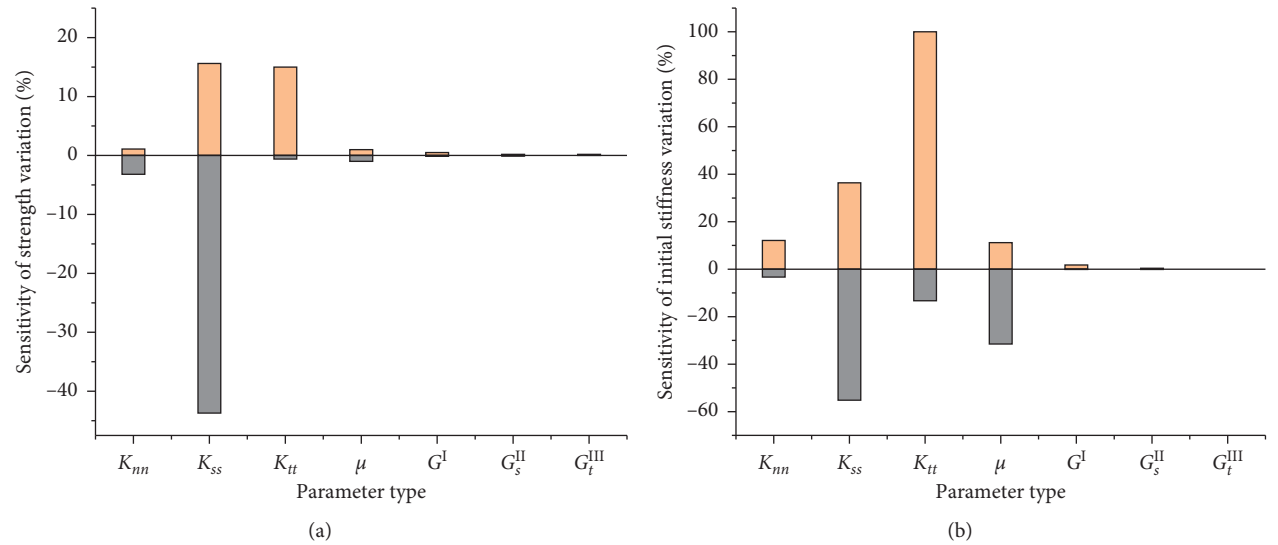

Figure 6: Sensitivity of structural response to modeling parameters. (a) Ultimate load. (b) Initial stiffness.

Table 4: The information and analysis results of infill walls with different aspect ratios.

Aspect ratio (H/L)	0.44			0.67			1.33		
Width (mm)	3658			2438			1220		
IP-IDR (%)	0	0.3	0.7	0	0.3	0.7	0	0.3	0.7
Stiffness (kN/mm × 10^3)	0.08	0.02	0.01	1.23	0.31	0.15	4.23	2.28	2.07
Ultimate load (kPa)	1.4	1.1	1.0	5.3	4.0	3.1	30.6	22.9	22.6

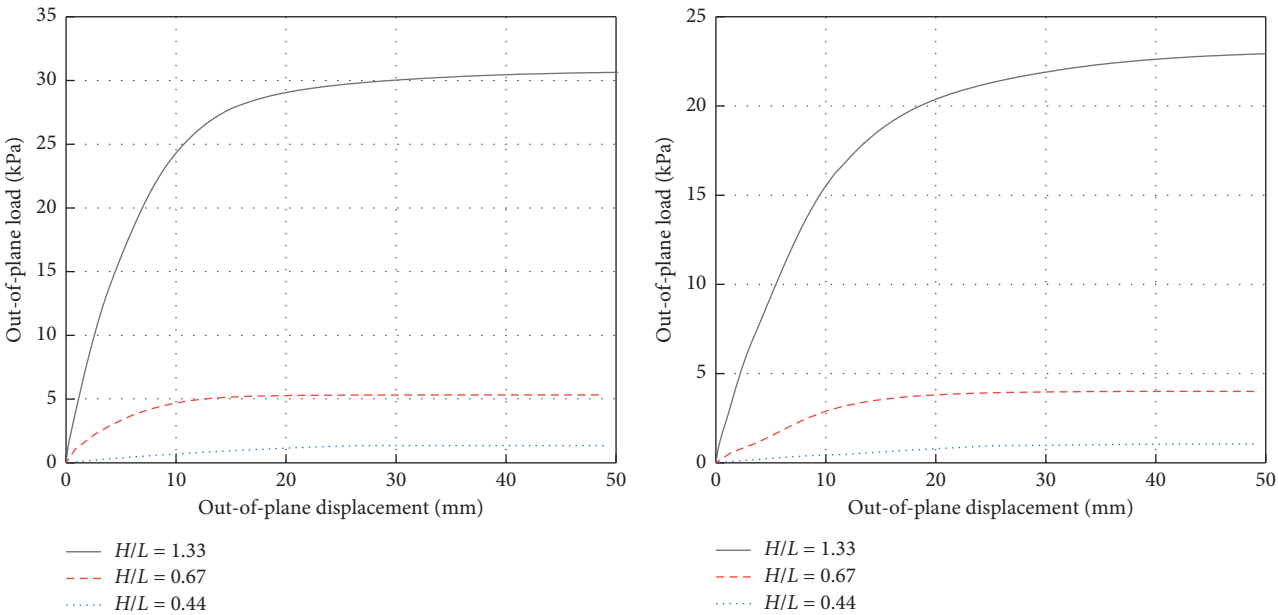

Figure 7: Continued.

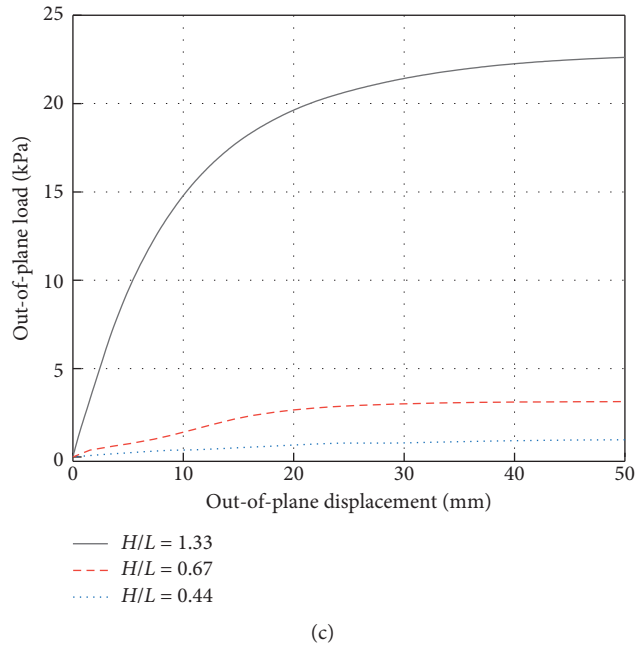

(c)

Figure 7: OOP load-displacement curves of infill walls with different aspect ratios. (a) Without IP damage. (b) With IP damage (IDR = 0.3%). (c) With IP damage (IDR = 0.7%).

the thickness of the infill wall. The height and width of all infill walls are 1625 mm and 2438 mm. Detailed information for different models is listed in Table 5. For each slenderness ratio, three analyses are conducted. The first is loaded in the OOP direction without IP damage. The other two correspond to OOP loading, with the IP-IDRs of 0.3% and 0.7% have been first reached, respectively. Similarly, nine analyses are conducted.

The stiffness and the ultimate load are obtained by using the same method as described above. The obtained stiffness and ultimate load are given in Table 5. The OOP load-displacement curves for each analyzed infilled model are described in Figure 8.

3.3. Effect of the Masonry Strength. In this part, infill walls with three different masonry strengths are analyzed, respectively. The values of masonry strength for analysis models are described in Table 6.

For each masonry strength, similar analyses with three different IP damage levels (without IP damage and IP-IDRs of 0.3% and 0.7%) are conducted. The obtained stiffness and ultimate load are listed in Table 6. Figure 9 shows the OOP load-displacement curves for analysis of infilled models with different IP damage levels.

4. Discussion of the Results

The relationship between the OOP ultimate load and stiffness with respect to the aspect ratio of infill walls with and without IP damage is presented in Figures 10(a) and 11(a), respectively. It is clear that the aspect ratio significantly influences the OOP performance of infilled frames. For the infill walls with a larger aspect ratio of 1.33 (the equal height and less span), the values of OOP ultimate load for different IDRs of 0, 0.3%, and 0.7% increase 577%, 573%, and 729%, compared with that of the infill wall with the aspect ratio of 0.67, and the values of stiffness increase 344%, 735%, and 1380%. The great increase of the ultimate load and stiffness should be attributed to the effect of the arching action that can play a larger role for smaller spans.

The ratio of the ultimate load and stiffness obtained for the IP damaged wall to the value obtained for the IP undamaged wall (i.e., R_f and R_K) is computed and reported with IP-IDR in Figures 10(b) and 11(b), respectively. It can be seen that the OOP performance is significantly affected by the IP damage level. As the IP damage increases, the OOP ultimate load and stiffness rapidly decrease. In addition, the aspect ratio also has the influence on the reduction of the OOP performance. At a given IP-IDR, the ultimate load and stiffness reduction are quite lower for the infills with smaller aspect ratio (with larger span).

The relationship between the OOP ultimate load and stiffness with respect to the slenderness ratio of infill walls with and without damage is presented in Figures 12(a) and 13(a), respectively. It can reflect the influence of the slenderness ratio on the OOP performances of infill walls. In particular, for larger slenderness ratio, the ultimate load and stiffness are reduced. To be specific, the values of ultimate load for different IDRs of 0%, 0.3%, and 0.7% increase 719%, 850%, and 1042%, and the values of stiffness increase 271%, 574%, and 627%, when the results of the infill wall with the slenderness ratio of 17 are compared to that with the slenderness ratio of 34. This can be attributed to the OOP arching action that thinner infill

Table 5: The information and analysis results of infill walls with different slenderness ratios.

Slenderness ratio (H/T)	17			26			34		
Thickness (mm)	96			63			58		
IP-IDR (%)	0	0.3	0.7	0	0.3	0.7	0	0.3	0.7
Stiffness (kN/mm × 10^3)	3.33	1.78	0.94	1.79	0.55	0.27	1.23	0.31	0.15
Ultimate load (kN)	38.1	34.0	32.3	10.6	7.8	7.2	5.3	4	3.1

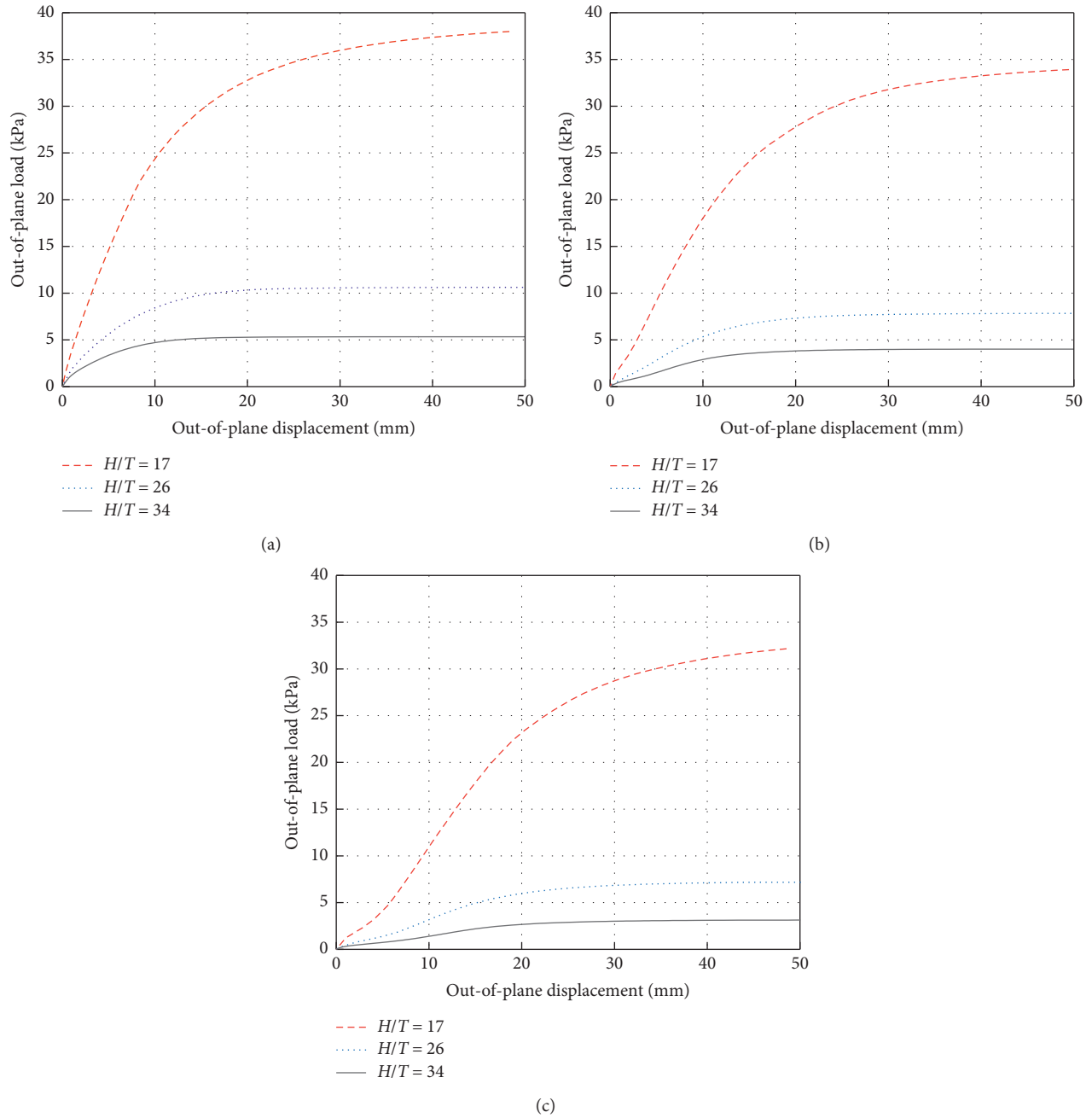

Figure 8: OOP load-displacement curves of infill walls with different slenderness ratios. (a) Without IP damage. (b) With IP damage (IDR = 0.3%). (c) With IP damage (IDR = 0.7%).

Table 6: The information and analysis results of infill walls with different masonry strengths.

Compressive strength of masonry (MPa)	4.9			10.9			16.9		
Tensile strength of masonry (MPa)	0.14			0.30			0.47		
Elastic modulus of masonry (GPa)	3.7			8.2			12.7		
IP-IDR (%)	0	0.3	0.7	0	0.3	0.7	0	0.3	0.7
Stiffness (kN/mm × 10^3)	0.88	0.23	0.14	1.23	0.31	0.15	1.34	0.35	0.17
Ultimate load (kN)	2.95	2.19	1.73	5.33	4.00	3.13	6.52	5.07	4.07

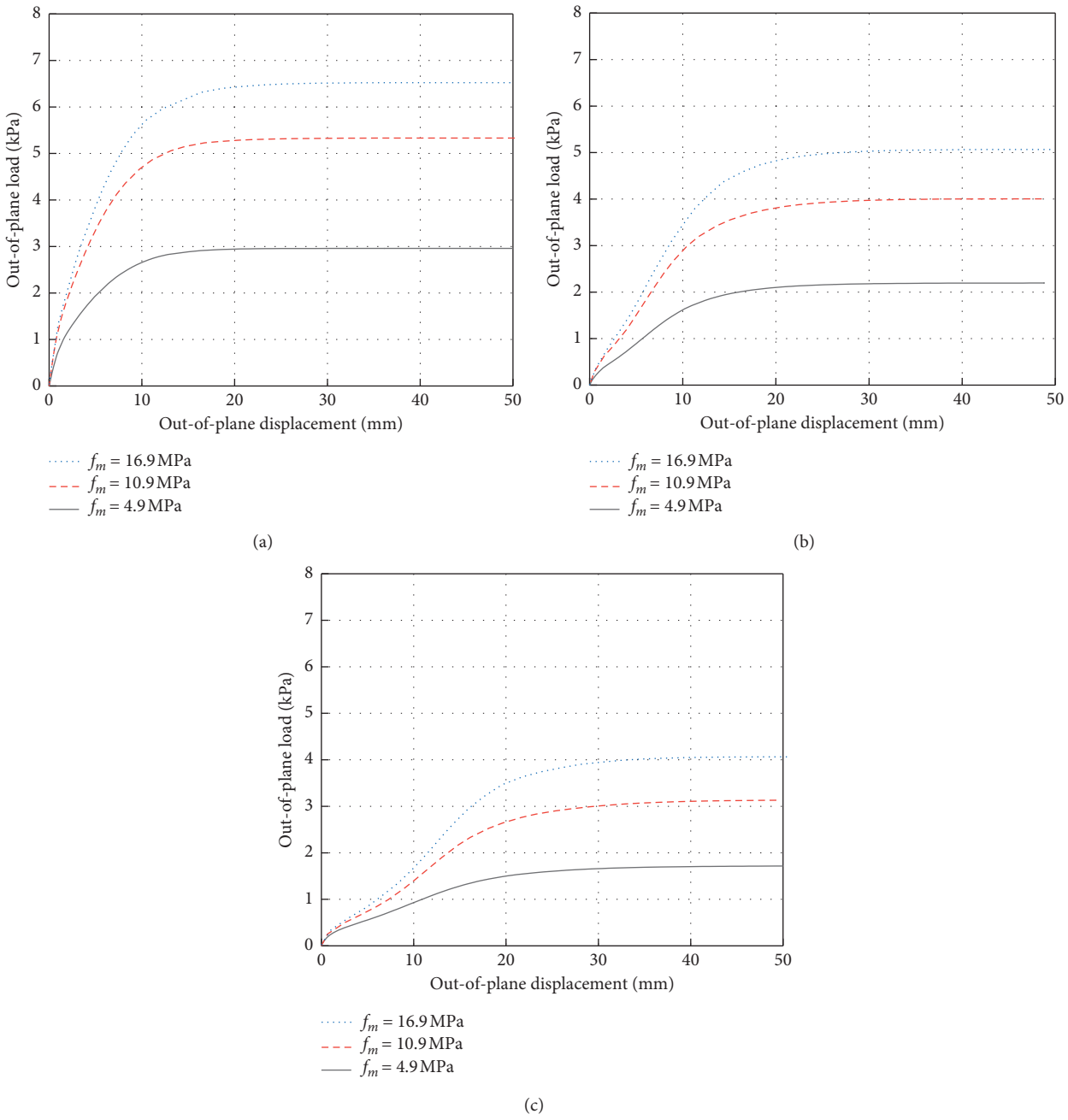

FIGURE 9: OOP load-displacement curves of infill walls with different masonry strengths. (a) Without IP damage. (b) With IP damage (IDR = 0.3%). (c) With IP damage (IDR = 0.7%).

wall is formed less obviously and the strength of masonry material is not fully utilized to resist loads. For the thicker infill wall, the contact between the wall and columns is larger and can provide more sufficient constrain to the OOP deformation of the infill wall. The ratio of the ultimate load and stiffness obtained for the IP damaged wall to the value obtained for the IP undamaged wall (i.e., R_f and R_K) is computed and reported with IP-IDR in Figures 12(b) and 13(b), respectively. It can be seen that the slenderness ratio significantly influences the IP and OOP interaction. At a given IP-IDR, the ultimate load and stiffness are significantly reduced for the infill walls with larger slenderness ratio (with thinner infill wall). Furthermore, it shows that the values of R_f and R_K for infill walls with slenderness ratios of 26 and 34 follow a similar trend, while a significant difference is observed for the values of the infill wall with a slenderness ratio of 17. The observation is consistent with the finding in the studies of Angel et al. [7] and Ricci et al. [14].

In Figures 14(a) and 15(a), the relationship between the OOP ultimate load and stiffness with respect to the masonry strength of infill walls with and without damage is presented.

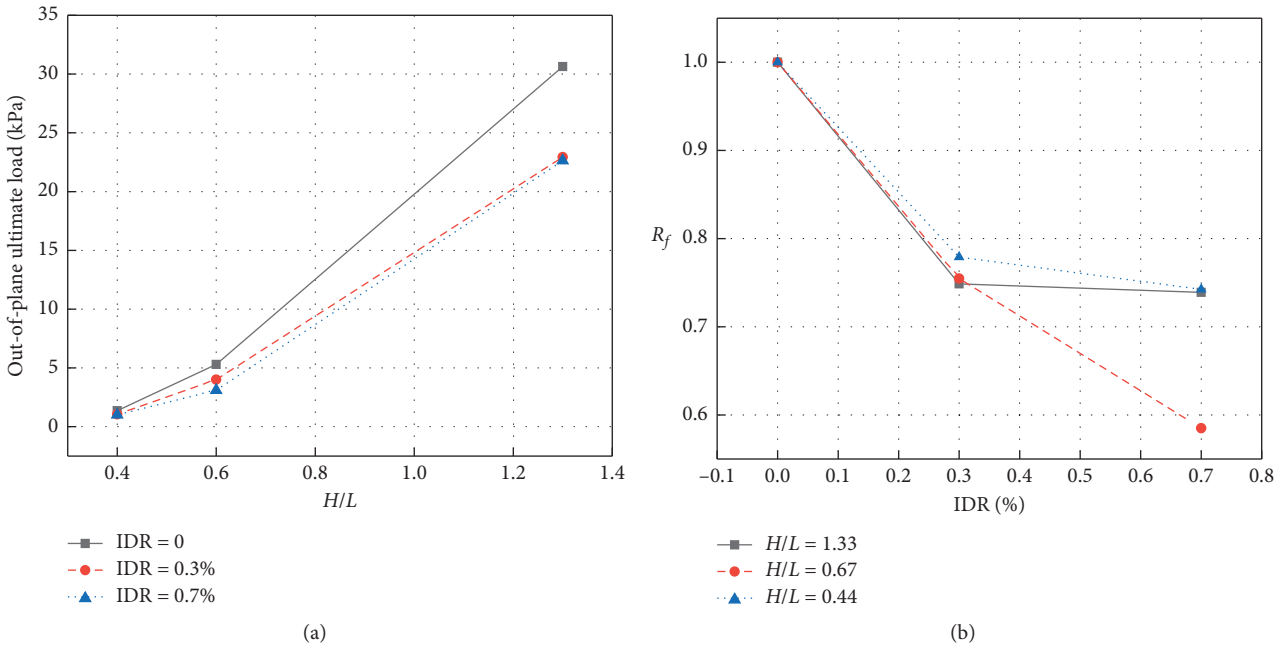

Figure 10: The effect (a) aspect ratio and (b) IP damage on the OOP strength of the infill wall.

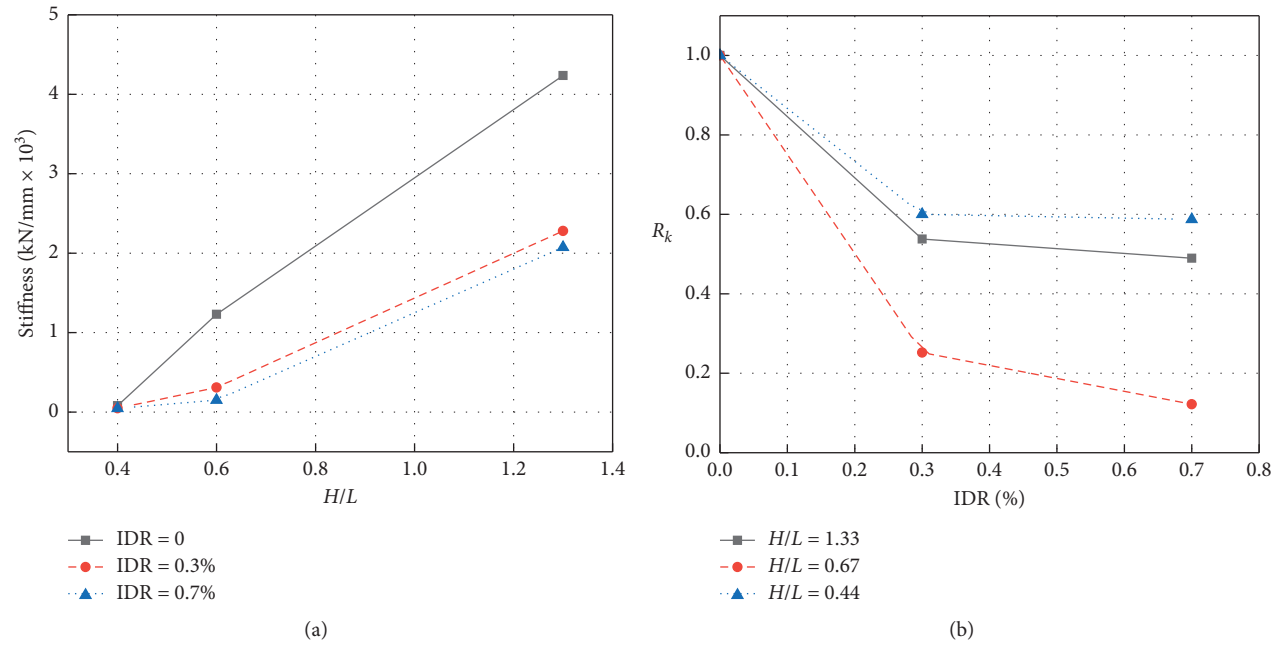

Figure 11: The effect of (a) aspect ratio and (b) IP damage on the OOP stiffness of the infill wall.

The ratio of the ultimate load and stiffness obtained for the IP damaged wall to the value obtained for the IP undamaged wall (i.e., R_f and R_K) is computed and reported with IP-IDR in Figures 14(b) and 15(b), respectively. It can be concluded that the masonry strength has a great influence on the OOP performance of infilled frames with and without IP damages. The increase of the masonry strength leads to the increase of both the ultimate load and stiffness. However, the influence of the masonry strength on the OOP ultimate load and stiffness reduction is not significant.

The analytical results are compared with value provided in the New Zealand code [35] and the prediction developed by Angel et al. [7], Ricci et al. [14], and Zizzo et al. [25] in Figure 16. The slenderness ratio plays a most important role on the interaction of IP and OOP performance of the infill wall. However, the influence of masonry strength and aspect ratio is not that obvious. The reduction factors of the infill wall with different slenderness ratios tend to approximate the value in the New Zealand code [35] with IDR increasing. In other words, the value provided by the New Zealand code

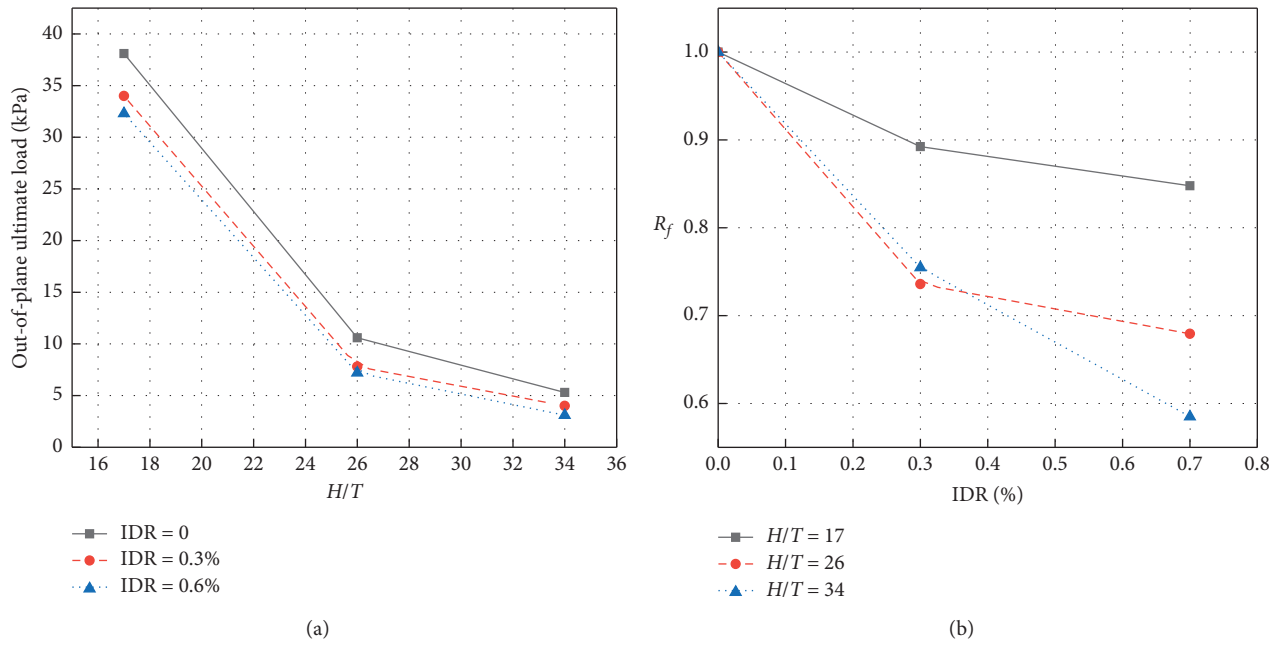

Figure 12: The effect of (a) slenderness ratio and (b) IP damage on the OOP strength of the infill wall.

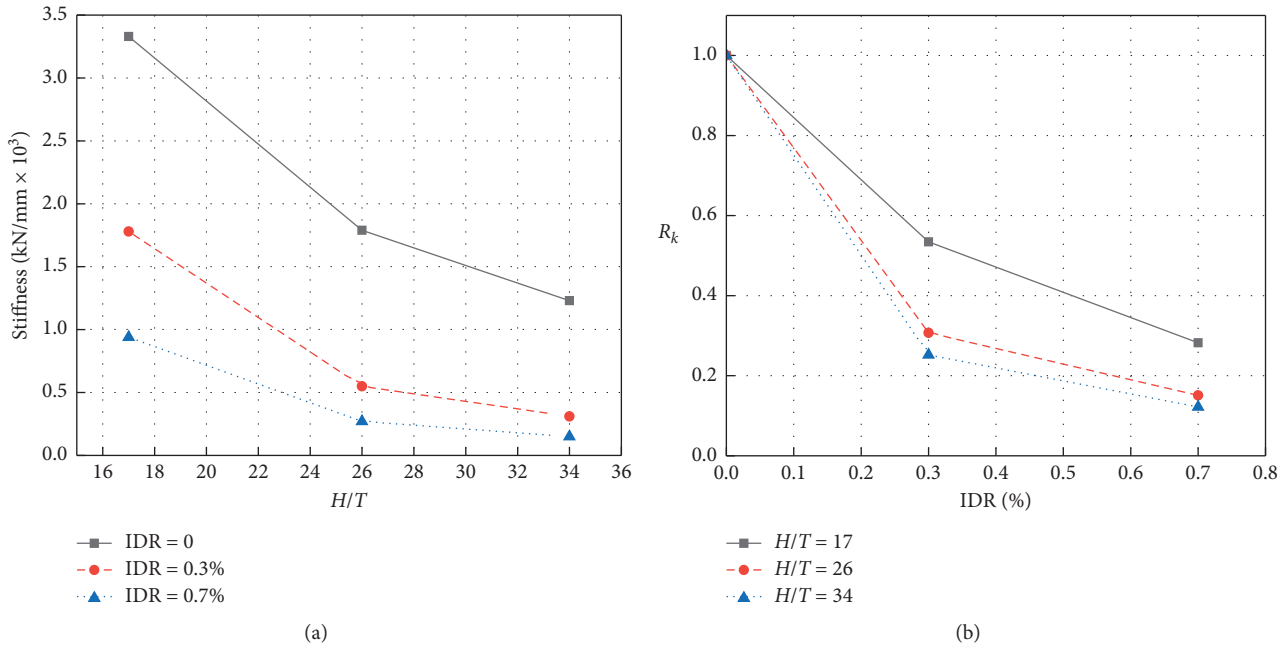

Figure 13: The effect (a) slenderness ratio and (b) IP damage on the OOP stiffness of the infill wall.

[35] is similar to the lower bound in this paper. However, the predictions in literatures [7, 14, 25] are quite different with the analytical result in this paper. This can be attributed to the experimental fact that the specimen without IP damage in the study of Angel et al. [7] is different from that with IP damage. The performance of the mortar in the specimen without IP damage is better comparing with that in the specimen with IP damage, which results in a higher ultimate load for the specimen without IP damage and a lower reduction ratio. However, the analytical models in this paper are exactly the same to each other. So the ultimate load without IP damage in this numerical investigation is lower than the experimental one, and the reduction ratio seems to be higher. Furthermore, the infill walls in literature [14, 25] are quite weak, and the masonry block will be damaged severely with relatively small IDR. However, the OOP behavior is influenced significantly by the IP masonry block damage. So, with a small IDR, the ultimate OOP load

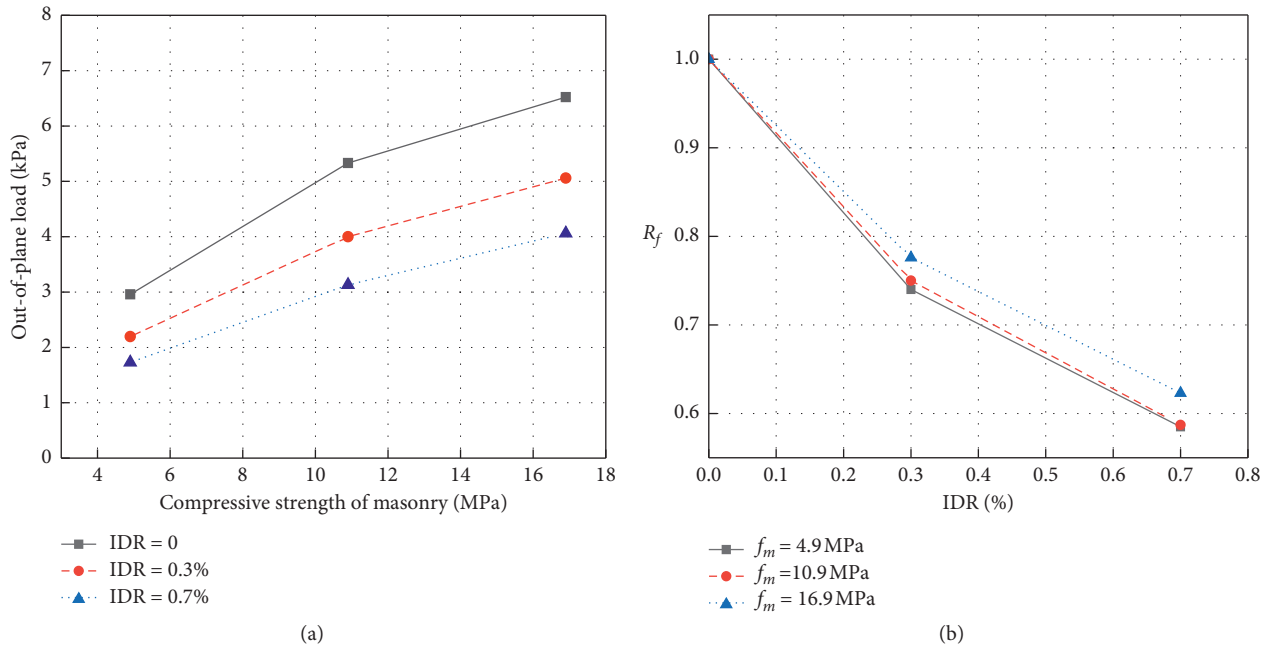

Figure 14: The effect (a) masonry strength and (b) IP damage on the OOP strength of the infill wall.

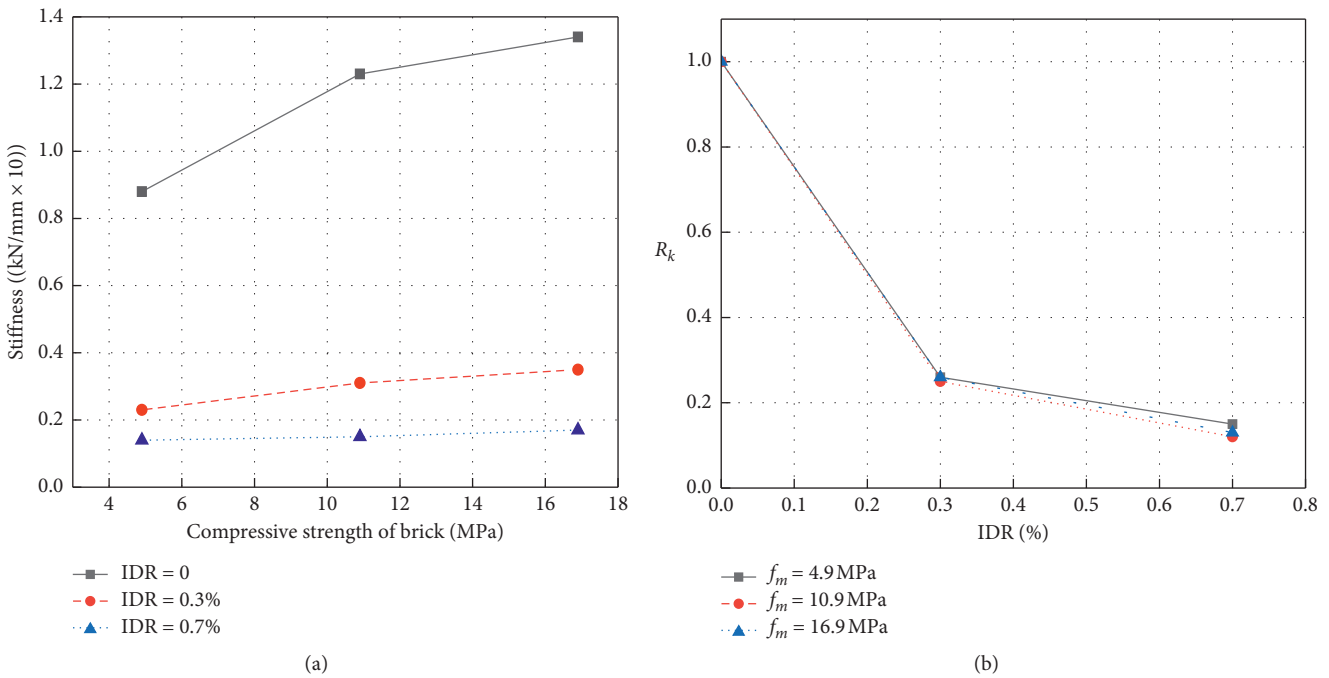

Figure 15: The effect (a) masonry strength and (b) IP damage on the OOP stiffness of the infill wall.

decreased obviously due to the severe IP damage, which results in a much lower reduction ratio.

5. Conclusions

This manuscript presents a 3D finite element modeling strategy to investigate OOP seismic behavior of masonry infill walls considering the existed IP damage. A numerical model for an experiment in the literature is established and calibrated. Then using the calibrated model as a reference, the effect of aspect ratio, slenderness ratio, and masonry strength on the IP and OOP interaction of infill walls is studied. Finally, the strength and stiffness reduction by the IP-IDR, considering the effect of aspect ratio, slenderness ratio, and masonry strength, is discussed. The following conclusions are drawn from this study:

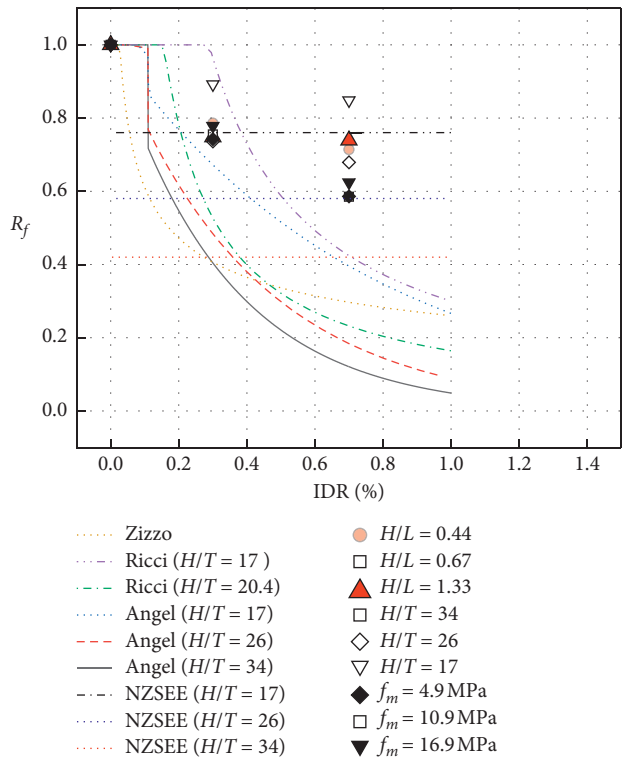

Figure 16: Comparison of the strength reduction factor of infill walls.

(1) The IP damage of the infill wall influences the OOP seismic performance significantly, including the OOP stiffness and ultimate load. The ultimate load will be decreased to less than 60% of the capacity of that only OOP loaded, as the result of the IP damage.

(2) The OOP load capacity and stiffness will be reduced due to the decrease of aspect ratio since the OOP arch action will get weak in the wider infill wall. The aspect ratio influences the reducing effect of the IP damage to the OOP seismic performance. So the aspect ratio should be considered in the evaluation of the effect of the IP damage in the future work.

(3) The OOP load capacity and stiffness will be reduced as there is increase in the slenderness ratio since the arching action does not form that well as the thicker infill wall. The effect of IP damage on the OOP seismic performance is more obvious due to the increase of the slenderness ratio.

(4) The masonry strength has a great influence on the OOP performance of infilled frames with and without IP damages. The increase of the masonry strength leads to the increase of both the ultimate load and stiffness. However, the influence of the masonry strength on the OOP ultimate load and stiffness reduction is not significant.

The work in this paper is the preliminary research. Since the OOP test is loading controlled, descending of load capacity cannot be obtained. Thus, the finite element model should be improved in the future. In addition, a simplified modeling technology should be proposed, which can simultaneously consider the IP and OOP seismic performance of infill walls. Thus, the behavior of infill walls in the earthquake event could be considered reasonably in the seismic analysis of RC frames.

Data Availability

The data of numerical results used to support the findings of this study can be obtained by contacting the corresponding author mailto: via email.

Conflicts of Interest

The authors declare that there are no conflicts of interest regarding the publication of this paper.

Acknowledgments

This investigation was supported by Scientific Research Fund of Institute of Engineering Mechanics, China Earthquake Administration (Grant Nos. 2018D15 and 2019D09), the National Nature Science Foundation of China (Nos. 51808478 and 51908484), and the Natural Science Foundation of Shandong (Nos. ZR2019QEE033 and ZR2019BEE039). These supports are greatly appreciated.

References

[1] F. G. Thomas, "The strength of brickwork," *Structural Engineering*, vol. 31, no. 2, pp. 35–46, 1953.

[2] E. L. Mc Dowell, K. E. Mc Kee, and E. Sevin, "Arching action theory of masonry walls," *Journal of the Structural Division*, vol. 82, no. 2, pp. 1–8, 1956.

[3] J. L. Dawe and C. K. Seah, "Out-of-plane resistance of concrete masonry infilled panels," *Canadian Journal of Civil Engineering*, vol. 16, no. 6, pp. 854–864, 1989.

[4] A. Dafnis, H. Kolsch, and H.-G. Reimerdes, "Arching in masonry walls subjected to earthquake motions," *Journal of Structural Engineering*, vol. 128, no. 2, pp. 153–159, 2002.

[5] Y. H. Tu, P. M. Liu, and H. P. Lin, "OOP seismic behavior of unreinforced masonry in-filled walls," in *Proceedings of the Structures Congress: New Horizons and Better Practices*, pp. 1–10, Long Beach, CA, USA, May 2007.

[6] Y.-H. Tu, T.-H. Chuang, P.-M. Liu, and Y.-S. Yang, "Out-of-plane shaking table tests on unreinforced masonry panels in RC frames," *Engineering Structures*, vol. 32, no. 12, pp. 3925–3935, 2010.

[7] R. Angel, D. P. Abrams, D. Shapiro, J. Uzarski, and M. Webster, "Behavior of reinforced concrete frames with masonry infills," Technical Report, University of Illinois Engineering Experiment Station. College of Engineering. University of Illinois at Urbana-Champaign., Urbana, Ill, USA, 1994.

[8] R. D. Flanagan and R. M. Bennett, "Bidirectional behavior of structural clay tile infilled frames," *Journal of Structural Engineering*, vol. 125, no. 3, pp. 236–244, 1999.

[9] R. D. Flanagan and R. M. Bennett, "Arching of masonry infilled frames: comparison of analytical methods," *Practice Periodical on Structural Design and Construction*, vol. 4, no. 3, pp. 105–110, 1999.

[10] G. M. Calvi and D. Bolognini, "Seismic response of reinforced concrete frames infilled with weakly reinforced masonry

panels," *Journal of Earthquake Engineering*, vol. 5, no. 2, pp. 153–185, 2001.

[11] J. S. Kuang and Y. P. Yuen, "Effect of OOP loading on IP behavior of unreinforced infilled RC frames," in *Proceedings of the International Conference on Computing in Civil and Building Engineering*, Nottinham, UK, June 2010.

[12] M. F. P. Pereira, M. F. N. Pereira, J. E. D. Ferreira, and P. B. Lourenco, "Behavior of masonry infill panels in RC frames subjected to in plane and out of plane loads," in *Proceedings of the 7th International Conference on Analytical Models and New Concepts in Concrete and Masonry Structures*, Krakow, Poland, June 2011.

[13] S. Hak, P. Morandi, and G. Magenes, "OOP experimental response of strong masonry infills," in *Proceedings of the European Conference on Earthquake Engineering and Seismology*, pp. 139–144, Istanbul, Turkey, June 2014.

[14] P. Ricci, M. Di Domenico, and G. M. Verderame, "Empirical-based out-of-plane URM infill wall model accounting for the interaction with in-plane demand," *Earthquake Engineering & Structural Dynamics*, vol. 47, no. 3, pp. 802–827, 2018.

[15] P. Ricci, M. Di Domenico, and G. M. Verderame, "Experimental investigation of the influence of slenderness ratio and of the in-plane/out-of-plane interaction on the out-of-plane strength of URM infill walls," *Construction and Building Materials*, vol. 191, no. 12, pp. 507–522, 2018.

[16] F. da Porto, G. Guidi, M. Dalla Benetta, and N. Verlato, "Combined IP/OOP experimental behaviour of reinforced and strengthened infill masonry walls," in *Proceedings of the 12th Canadian Masonry Symposium*, Vancouver, Canada, June 2013.

[17] M. T. de Risi, M. Di Domenico, P. Ricci, G. M. Verderame, and G. Manfredi, "Experimental investigation on the influence of the aspect ratio on the in-plane/out-of-plane interaction for masonry infills in RC frames," *Engineering Structures*, vol. 189, no. 6, pp. 523–540, 2019.

[18] O. Rabinovitch and H. Madah, "Finite element modeling and shake-table testing of unidirectional infill masonry walls under out-of-plane dynamic loads," *Engineering Structures*, vol. 33, no. 9, pp. 2683–2696, 2011.

[19] C.-H. Zhai, J.-C. Kong, X.-M. Wang, and X.-H. Wang, "Finite-element analysis of out-of-plane behaviour of masonry infill walls," *Proceedings of the Institution of Civil Engineers —Structures and Buildings*, vol. 171, no. 3, pp. 203–215, 2018.

[20] A. Mohyeddin, H. M. Goldsworthy, and E. F. Gad, "FE modelling of RC frames with masonry infill panels under in-plane and out-of-plane loading," *Engineering Structures*, vol. 51, pp. 73–87, 2013.

[21] Y. P. Yuen and J. S. Kuang, "Masonry-infilled rc frames subjected to combined in-plane and out-of-plane loading," *International Journal of Structural Stability and Dynamics*, vol. 14, no. 02, p. 1350066, 2014.

[22] G. M. Mohammadi, "Out of plane strength of infill panels," in *Proceedings of the 14th World Conference on Earthquake Engineering*, Beijing, China, October 2008.

[23] N. Verlato, G. Guidi, and F. da Porto, "Experimental testing and numerical modelling of infill masonry walls subjected to IP damage," in *Proceedings of the Second European Conference on Earthquake Engineering and Seismology*, pp. 25–29, Istanbul, Turkey, August 2014.

[24] P. Agnihotri, V. Singhal, and D. C. Rai, "Effect of in-plane damage on out-of-plane strength of unreinforced masonry walls," *Engineering Structures*, vol. 57, pp. 1–11, 2013.

[25] M. Zizzo, L. Cavaleri, and F. Di Trapani, "Out of plane capacity of infills after in plane loading: a prediction analytical model," in *Proceedings of theCOMPDYN 2019 7th ECCOMAS Thematic Conference on Computational Methods in Structural Dynamics and Earthquake Engineering*, Crete, Greece, June 2019.

[26] S. Kadysiewski and K. M. Mosalam, "Modeling of Unreinforced Masonry Infill Walls Considering IP and OOP interaction," in *Proceedings of the 11th Canadian Masonry Symposium*, Toronto, Ontario, June 2009.

[27] K. M. Mosalam and S. Günay, "Progressive collapse analysis of reinforced concrete frames with unreinforced masonry infill walls considering in-plane/out-of-plane interaction," *Earthquake Spectra*, vol. 31, no. 2, pp. 921–943, 2015.

[28] A. Furtado, H. Rodrigues, A. Arêde, and H. Varum, "Simplified macro-model for infill masonry walls considering the out-of-plane behaviour," *Earthquake Engineering & Structural Dynamics*, vol. 45, no. 4, pp. 507–524, 2016.

[29] A. Furtado, H. Rodrigues, A. Arêde, and H. Varum, "Influence of the in plane and out-of-plane masonry infill walls' interaction in the structural response of RC buildings," *Procedia Engineering*, vol. 114, pp. 722–729, 2015.

[30] F. Di Trapani, P. B. Shing, and L. Cavaleri, "Macroelement model for IP and OOP responses of masonry infills in frame structures," *Journal of Structural Engineering*, vol. 144, no. 2, Article ID 04017198, 2018.

[31] P. Morandi, S. Hak, and G. Magenes, "Simplified OOP resistance verification for slender clay masonry infills in RC frames," in *Proceedings of the XV ANIDIS, L'Ingegneria Sismica in Italia*, Padua, Italy, July 2013.

[32] M. Pasca, L. Liberatore, and R. Masiani, "Reliability of analytical models for the prediction of OOP capacity of masonry infills," *Structural Engineering and Mechanics*, vol. 64, no. 6, pp. 765–781, 2017.

[33] P. B. Lourenço and J. G. Rots, "Multisurface interface model for analysis of masonry structures," *Journal of Engineering Mechanics*, vol. 123, no. 7, pp. 660–668, 1997.

[34] G. Q. Liu, *The Research on the Basic Mechanical Behavior of Masonry structure*, Hunan University, Changsha, China, 2005, in Chinese.

[35] NZSEE 2017. New Zealand Society for Earthquake Engineering (NZSEE), Structural Engineering Society New Zealand Inc. (SESOC), New Zealand geotechnical society inc., Ministry of business, innovation and employment, earthquake commission. The Seismic Assessment of Existing Buildings (The Guidelines), Part C – Detailed Seismic Assessment, 2017.